# A Probabilistic Measure of Multi-Robot Connectivity and Ergodic Optimal Control

Yongce Liu[1], Zhongqiang Ren[1,2]
[1]UM-SJTU Joint Institute, [2]Department of Automation
Shanghai Jiao Tong University, Shanghai, China
Email: {yongce.liu, zhongqiang.ren}@sjtu.edu.cn

***Abstract*—This paper considers multi-robot trajectory planning for information gathering with intermittent connectivity maintenance. For information gathering, ergodic search provides a framework to inherently balance between exploration (visit all locations for information) and exploitation (greedily search high information regions), by planning trajectories such that the amount of time the robots spend in a region is proportional to the amount of information in that region. Although ergodic search was studied in different ways, most of them ignore or over-simplify the connectivity maintenance requirement among the robots, which is crucial for information exchange in missions without global communication. This paper introduces a novel probabilistic measure of inter-robot connectivity based on the time-averaged statistics of the robots' trajectories. Such a measure provides a new way to impose intermittent connectivity constraints during the ergodic search, which leads to an optimal control problem (OCP). We derive the theoretical condition for optimality based on the Pontryagin principle, and develop iLQR and augmented Lagrangian methods to numerically solve this OCP. Our experimental results validate the effectiveness of the proposed probabilistic measure and demonstrate that the ergodic search combined with this measure achieves better ergodic metrics compared to baseline approaches. We also demonstrate our planner on a multi-drone system.[1]**

## I. Introduction

This paper investigates a multi-robot trajectory planning problem for information gathering while maintaining intermittent connectivity among the robots, which arises in applications such as exploration [1] and search and rescue [2]. Given an information map, a probability distribution describing the information density at each location over the area to be searched, this paper aims to plan trajectories for the robots to gather information from this map and establish the robot-robot connection when needed to exchange information. Existing approaches for information collection range from complete coverage [3, 4] that uniformly and systematically covers the area, to information-theoretic approaches [5, 6] that greedily direct the robot to the next location with the highest information gain. Different from them, ergodic search [7–9] provides an approach that can inherently balance between exploitation (greedily moving to high-information areas) and exploration (visiting all possible locations). Ergodic search plans trajectories by minimizing an ergodic metric (ergodicity) so that the time spent in any region is proportional to a measure of information in that region.

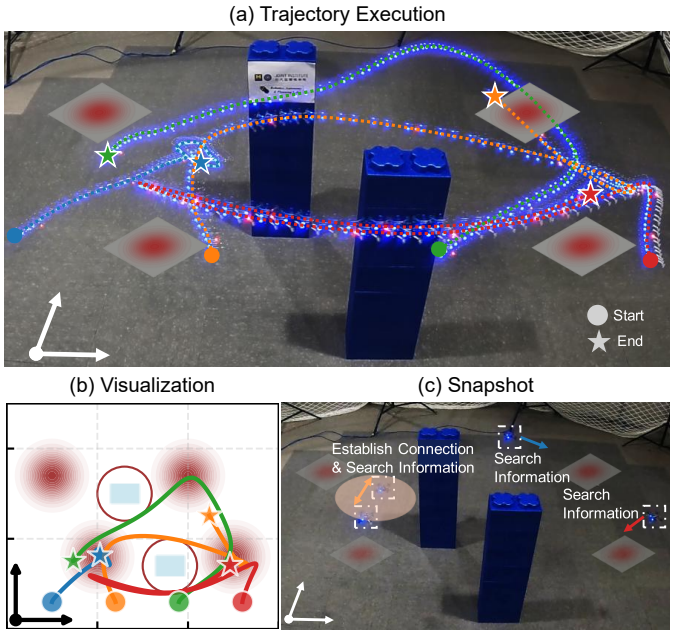


Fig. 1. Multi-robot ergodic search with intermittent connectivity. (a): Multiple drones plan ergodic trajectories among obstacles to explore a map characterized by information distribution while maintaining intermittent pairwise connectivity. The robots have to balance between information gathering (evaluated via the ergodic metric) and connectivity maintenance. (b): The top-down view of the map and the trajectories. (c): A snapshot during the trajectory execution, where drones are establishing connections and searching for information.

Although multi-robot ergodic search has been investigated a lot [10–14], most of them either ignores the limited connectivity among robots [10, 11], assuming all robots are connected with a central communication hub at all times [12, 13], or require all robots to stay connected with pre-determined and fixed connection topology [14]. This paper aims to let the robots determine flexibly when and where to establish connections during the ergodic search, and thus has the potential to achieve better ergodicity.

Multi-robot information collection with connectivity maintenance has been investigated [15–20], and the challenge is to determine when and where the robots should meet and what topology of the connection should be formed. In general,

[1]This work was supported by the Natural Science Foundation of Shanghai under Grant 24ZR1435900, and the Natural Science Foundation of China under Grant 62403313. (Corresponding author: Zhongqiang Ren.) Our code is available at https://github.com/rap-lab-org/public_pymec.

connectivity maintenance and information collection are two competitive objectives in the sense that maintaining connectivity often lowers the efficiency of information collection, especially when the information is widely distributed over the workspace and the robots have to deviate from their optimal trajectories for information collection to build inter-robot connections. To balance these two competitive objectives, instead of maintaining the connection at all times [21–24], requiring intermittent connection with either fixed periods [17] or computed connection schedules [18–20] can help improve the efficiency of information collection.

The idea of maintaining connectivity during ergodic search in this paper belongs to the broad category of intermittent connectivity, yet in a soft manner. Unlike existing approaches to maintain intermittent connection, such as planning reconnection paths [16], searching for other robots to establish connections [25], sampling feasible connection paths [17], or scheduling discrete connection events [18–20], we introduce a novel probabilistic measure for characterizing inter-robot connectivity based on the time-averaged statistics of robot trajectories. The proposed measure attempts to avoid explicitly formulating the connection locations, times, and topologies as the planning objective or constraints, or imposing any hard constraints on connectivity. Instead, this paper seeks to infer the probability of connection among the robots based on the distribution of their trajectories as the time horizon goes to infinity. Such a measure provides a way to impose intermittent connectivity constraints as soft constraints for trajectory optimization, and allows us to formulate a corresponding optimal control problem (OCP) that considers both ergodic search and connectivity maintenance. To solve this OCP, in theory, we show how to rewrite this OCP into a standard Bolza form, and derive the condition for optimality based on the Pontryagin principle. In practice, we provide an algorithm based on the augmented Lagrangian method (ALM) and iterative linear quadratic regulator (iLQR) that can numerically solve the OCP.

Our experimental results verify the effectiveness of the proposed probabilistic measure, as we observe a positive correlation between the value of the measure and the actual connection time between the robots along their planned trajectories. Additionally, the results show that the ergodic search combined with our measure achieves better ergodic metrics than the baseline approaches, and the robots can intelligently balance between ergodic search and connectivity maintenance in the long run. Finally, we showcase the use of our planner on a multi-drone system in a lab setting.

## II. Related Work

### A. Ergodic Search

Ergodic search optimizes robot trajectories by minimizing the difference between the time-averaged statistics of the robot's path and the desired information distribution within a workspace. To quantify this difference, researchers have developed various optimization metrics. Among them, spectral multi-scale coverage (SMC) [7] employs Fourier decomposition to measure the difference. Kullback-Leibler (KL) divergence metric [26] approximates the robot's spatial distribution using a Gaussian mixture model. Kernel ergodic metric [27] extends ergodic search from Euclidean space to Lie groups in a computationally efficient way. The ergodic maximum mean discrepancy metric [28] samples from the search domain to define the metric and plan ergodic trajectories.

Gradient-based methods are commonly employed to plan ergodic trajectories by optimizing the ergodic metric. These approaches include feedback control laws for both first-order and second-order dynamics in [7], receding-horizon ergodic exploration [12], the ergodicity-based coverage algorithm via a potential field [29], the application of differential dynamic programming (DDP) [9], and iterative optimization using linear quadratic regulator (LQR) [8].

The scope of ergodic search has recently expanded to encompass various optimization objectives, including time optimality [30], multi-objective optimization [10], and energy efficiency [31]. The practical applications of ergodic control have also diversified, spanning robotic insertion tasks [32], preserving flows measurement [33], and real-time area coverage and target localization applications [12, 13].

### B. Connectivity Maintenance

Connectivity maintenance was extensively studied. Continual connectivity requires all robots to stay connected at all times globally [21–23] or locally [24], which is suitable for communication-critical missions. Periodic connectivity [17] requires all robots to regain connectivity at pre-defined fixed intervals. Intermittent connectivity [18–20] enables the robots to meet at some locations intermittently over time without enforcing a fixed time interval between two subsequent connections, demonstrating higher flexibility.

Various approaches have been studied to maintain intermittent connectivity. Some methods focus on selecting connection times or locations, such as searching other robots for connection [25], choosing rendezvous locations [34], planning reconnection paths with minimum travel cost [16], and determining connection times and locations using integer linear programming (ILP) [15]. Other work seeks to first determine the connection schedule and then plan the trajectories based on the schedules [18–20].

This paper aims to maintain intermittent connectivity during ergodic search. Given these advances in intermittent connectivity maintenance, most existing methods cannot be directly applied to ergodic search, since many connectivity maintenance approaches involve discrete task planning [25, 34] or sampling-based methods [17, 18], which are challenging to integrate with gradient-based trajectory optimization for ergodic search since the optimization objective (i.e., the ergodic metric) is defined over the entire trajectory. Additionally, ergodic trajectory planning studies the statistical behaviors of dynamical systems in the long run, and investigating inter-robot connectivity based on the statistical behaviors of the dynamical systems may provide a new planning framework to intelligently balance between connectivity maintenance and ergodicity of the system in the long run.

## III. Preliminaries

### A. Notations

Let $\mathcal{W} = [0, L_1] \times \cdots \times [0, L_\nu] \subset \mathbb{R}^\nu, \nu \in \{1, 2, 3\}$ denote the workspace for all robots, where $L_\nu \in \mathbb{R}^+$ is the bound for the $\nu$-th dimension of the workspace $\mathcal{W}$. Let $w \in \mathcal{W}$ represent a point (location) in the workspace. Let $t \in [0, T]$ denote the time variable, where $T \in \mathbb{R}^+$ represents the planning time horizon. Let $I_N = \{1, 2, \cdots, N\}$ represent the set of robots, and superscripts such as $i, j$ on variables denote the associated robot. Additionally, let $\mathcal{R} = \{(i, j) \mid i, j \in I_N, i \neq j\}$ denote the set of enumerated robot pairs.

Each robot $i \in I_N$ has a state $x^i(t) \in \mathcal{X}$, control input $u^i(t) \in \mathcal{U}$, and location $q^i(t) \in \mathcal{W}$, where $\mathcal{X} \subset \mathbb{R}^n$ and $\mathcal{U} \subset \mathbb{R}^m$ denote the state space and control space, respectively. Furthermore, let $x(t) = (x^1(t), \cdots, x^N(t)) \in \mathcal{X}^N = \mathcal{X} \times \cdots \times \mathcal{X}$, $u(t) = (u^1(t), \cdots, u^N(t)) \in \mathcal{U}^N = \mathcal{U} \times \cdots \times \mathcal{U}$, and $q(t) = (q^1(t), \cdots, q^N(t)) \in \mathcal{W}^N = \mathcal{W} \times \cdots \times \mathcal{W}$ denote the joint state, joint control, and joint location column vectors, respectively. Finally, let $\dot{x}(t) = f(x(t), u(t))$ denote the joint dynamics of all robots. For notational simplicity, $x$, $u$, and $q$ represent the entire trajectories over $[0, T]$ in this paper.

### B. Ergodic Metric

Let $\phi(w) : \mathcal{W} \to \mathbb{R}_0^+$ denote a time-invariant probability distribution function such that $\int_{\mathcal{W}} \phi(w) dw = 1$, which describes the information density at each location across the workspace $\mathcal{W}$. Based on the trajectory $q^i$, the time-averaged statistics for robot $i \in I_N$ is defined as follows [7].

$$c^i(w) = c(w, q^i) = \frac{1}{T} \int_0^T \delta(w - q^i(t)) dt \tag{1}$$

where $\delta(w)$ is the Dirac delta function such that $\delta(\mathbf{0}) = +\infty$ and $\delta(w) = 0, w \neq \mathbf{0}$, satisfying $\int_{\mathbb{R}^\nu} \delta(w) dw = 1$. Note that $\int_{\mathcal{W}} c^i(w) dw = 1$ as $q^i(t) \in \mathcal{W}, \forall t \in [0, T]$.

With $\phi(w)$ and $c^i(w)$, the ergodic metric (ergodicity) for all robots is defined as the difference between the time-averaged statistics of all the robots and the information distribution map in the Fourier coefficient space as follows [7].

$$\mathcal{E}(\phi, q) = \sum_{\mathbf{k} \in \mathcal{K}} \Lambda_{\mathbf{k}} \left( \frac{1}{N} \sum_{i \in I_N} c^i_{\mathbf{k}} - \phi_{\mathbf{k}} \right)^2 \tag{2}$$

$$= \sum_{\mathbf{k} \in \mathcal{K}} \Lambda_{\mathbf{k}} \left( \frac{1}{NT} \sum_{i \in I_N} \int_0^T F_{\mathbf{k}}(q^i(t)) dt - \int_{\mathcal{W}} \phi(w) F_{\mathbf{k}}(w) dw \right)^2$$

Here, $c^i_{\mathbf{k}}$ and $\phi_{\mathbf{k}}$ are the Fourier coefficients of $c^i(w)$ and $\phi(w)$, respectively. $\mathbf{k} = (k_1, \cdots, k_\nu) \in \mathcal{K}$ is the frequency vector of the Fourier coefficients, and $\mathcal{K} \subset \mathbb{N}^\nu$ represents a selected set of frequencies in practical computation. Besides, $F_{\mathbf{k}}(w) = \frac{1}{h_{\mathbf{k}}} \prod_{m=1}^{\nu} \cos\left(\frac{k_m \pi}{L_m} w_m\right)$ is the cosine basis function with the normalization term $h_{\mathbf{k}}$ [7, 30, 35]. $\Lambda_{\mathbf{k}} = (1 + \| \mathbf{k} \|_2^2)^{-(\nu+1)/2}$ is the weight of each Fourier coefficient.

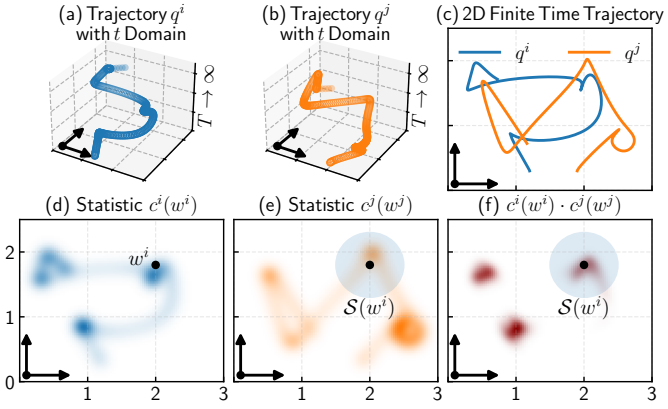


Fig. 2. Visualization of the connection probability. (a)-(b): The trajectories $q^i(t), q^j(t)$ of robots $i, j$ with time $t$ represented as the $z$-axis. (c): The top-down view of the trajectories of robots $i, j$. (d)-(e): The corresponding time-averaged statistics $c^i$ and $c^j$ represented as heatmaps. (f): The joint distribution heatmap ($c^i \cdot c^j$).

## IV. Probabilistic Measure of Connectivity

This section first defines the concepts related to the new probabilistic measure of connectivity between a pair of robots, and then discusses the intuition behind the measure.

### A. Connection Probability

We define the *connection area* $\mathcal{S}(w) \subset \mathbb{R}^\nu$ for a location $w \in \mathcal{W}$ as follows. Robot $j$ is connected with robot $i$ at time $t$ if robot $j$'s location $q^j(t)$ lies within robot $i$'s connection area $\mathcal{S}(q^i(t))$ (i.e., $q^j(t) \in \mathcal{S}(q^i(t))$). In this paper, we assume the connectivity between robots is bidirectional:

**Assumption 1** (Bidirectional Connectivity)**.**
*If $q^j(t) \in \mathcal{S}(q^i(t))$, then $q^i(t) \in \mathcal{S}(q^j(t))$.*

An example choice of $\mathcal{S}(w)$ that satisfies the bidirectional connectivity assumption is a circular region centered at $w$ with a fixed radius that remains constant across all robots (Fig. 2).

Intuitively, Eq. (1), i.e., the time average statistics $c^i(w^i)$ of a trajectory $q^i$, describes the percentage of time that $q^i$ stays at a location $w^i \in \mathcal{W}$ within the time horizon $T$. When $T$ goes to infinity, $c^i(w^i)$ describes the spatial distribution of robot $i$ in the workspace. Specifically, let

$$c^i_\infty(w^i) = \lim_{T \to \infty} c^i(w^i) = \lim_{T \to \infty} \frac{1}{T} \int_0^T \delta(w^i - q^i(t)) dt \tag{3}$$

denote the *spatial distribution* of robot $i$ over an infinite time horizon, which indicates the likelihood that robot $i$ appears at location $w^i$ over an infinite time horizon.

Leveraging the spatial distributions of two robots, we can infer the likelihood that the two robots are connected within the infinite time horizon. We introduce a probabilistic measure of connectivity between any pair of robots $(i, j) \in \mathcal{R}$ as:

**Definition 1** (Connection Probability (CP)). *Let $P_\infty(q^i, q^j)$ denote the connection probability:*

$$P_\infty(q^i, q^j) = \int_{w^i \in \mathcal{W}} \int_{w^j \in \mathcal{S}(w^i)} c^i_\infty(w^i) c^j_\infty(w^j) dw^j dw^i \quad (4)$$

The trajectories $q^i$ and $q^j$ are independent since each robot has its own control and dynamics. As a result, the spatial distributions $c^i(w^i)$ and $c^j(w^j)$ of robots $i, j$ are also independent from each other. Note that $\int_{\mathcal{W}} \int_{\mathcal{W}} c^i_\infty(w^i) c^j_\infty(w^j) dw^j dw^i = 1$, and the product $c^i_\infty(w^i) c^j_\infty(w^j)$ represents the joint probability density of robots $i$ and $j$ being at locations $w^i$ and $w^j$ respectively (not necessarily at the same time instant). Besides, $P_\infty(q^i, q^j)$ computes the cumulative distribution over all possible locations $w^i \in \mathcal{W}$ and $w^j \in \mathcal{S}(w^i)$, measuring the probability that robot $j$ lies within robot $i$'s connection area $\mathcal{S}(q^i(t^i))$ at any time $t^i$ over the infinite time horizon $[0, \infty)$.

**Theorem 1.** *Given the Assumption 1, the connection probability is symmetric, i.e., $P_\infty(q^i, q^j) = P_\infty(q^j, q^i)$.*

*Proof.* The proof is provided in Appendix A-A. □

### B. Finite Time Formulation

It is noted that Eq. (4) provides a meaningful probabilistic interpretation when $T$ approaches infinity (as opposed to a finite $T$). When $T$ approaches infinity, $c^i_\infty$ characterizes the spatial distribution of robot $i$, while $P_\infty(q^i, q^j)$ quantifies the connection probability between robots $i$ and $j$.[2] However, planning over an infinite time horizon is impractical in real-world applications. Hence, we introduce a finite-time approximation of Eq. (4) as:

**Definition 2** (Finite-Time Approximation). *Let $P_c(q^i, q^j; 0, T)$ denote the finite-time approximated connection probability (FCP), where the subscript $c$ in $P_c$ stands for "connection".*

$$\begin{aligned}
P_c(q^i, q^j; 0, T) &= \int_{w^i \in \mathcal{W}} \int_{w^j \in \mathcal{S}(w^i)} c^i(w^i) c^j(w^j) dw^j dw^i \\
&= \int_{w^i \in \mathcal{W}} \int_{w^j \in \mathcal{S}(w^i)} \Big( \frac{1}{T} \int_0^T \delta(w^i - q^i(t^i)) dt^i \\
&\qquad \frac{1}{T} \int_0^T \delta(w^j - q^j(t^j)) dt^j \Big) dw^j dw^i \\
&= \frac{1}{T^2} \int_0^T \int_0^T \Big( \int_{w^i \in \mathcal{W}} \int_{w^j \in \mathcal{S}(w^i)} \delta(w^i - q^i(t^i)) \\
&\qquad \delta(w^j - q^j(t^j)) dw^j dw^i \Big) dt^j dt^i \quad (5a) \\
&= \frac{1}{T^2} \int_0^T \int_0^T \gamma(q^i(t^i), q^j(t^j)) dt^j dt^i \quad (5b)
\end{aligned}$$

[2]Although the connection between robots requires them to be at specific locations at the *same time*, the connection probability focuses on their spatial distributions while relaxing the temporal simultaneity requirement. It is investigated in our experiments in Sec. VII-D how this relaxation affects the connection establishment in practice. We also derive the formulation considering simultaneity in Sec. VII-E for comparison.

where the *Connection Indicator Function (CIF)* $\gamma(w^i, w^j) : \mathcal{W} \times \mathcal{W} \to \{0, 1\}$ is defined as:

$$\gamma(w^i, w^j) = \begin{cases} 1 & w^j \in \mathcal{S}(w^i) \\ 0 & \text{otherwise} \end{cases} \quad (6)$$

The transition from Eq. (5a) to (5b) is explained in the next paragraph. Here, $P_c(q^i, q^j; 0, T) \in [0, 1]$. Specifically, for $\forall t^i, t^j \in [0, T]$, $P_c(q^i, q^j; 0, T) = 0$ if $\gamma(q^i(t^i), q^j(t^j)) = 0$, and $P_c(q^i, q^j; 0, T) = 1$ if $\gamma(q^i(t^i), q^j(t^j)) = 1$. For example, when robot $i$ stays at a stationary location $\tilde{q}^i \in \mathcal{W}$, i.e., $q^i(t^i) = \tilde{q}^i, \forall t^i \in [0, T]$, then $P_c(q^i, q^j; 0, T) = 1$ if $q^j(t^j) \in \mathcal{S}(\tilde{q}^i), \forall t^j \in [0, T]$.

To bridge the transition from Eq. (5a) to (5b), we define the CIF (6). For any given time points $t^i, t^j \in [0, T]$, we can rewrite the internal double integral in Eq. (5a) as follows:

$$\begin{aligned}
&\int_{w^i \in \mathcal{W}} \int_{w^j \in \mathcal{S}(w^i)} \delta(w^i - q^i(t^i)) \delta(w^j - q^j(t^j)) dw^j dw^i \\
&= \int_{w^i \in \mathcal{W}} \delta(w^i - q^i(t^i)) \int_{w^j \in \mathcal{S}(w^i)} \delta(w^j - q^j(t^j)) dw^j dw^i \\
&= \begin{cases} 1 & \text{if } q^j(t^j) \in \mathcal{S}(q^i(t^i)) \\ 0 & \text{otherwise} \end{cases} \quad (7)
\end{aligned}$$

By the properties of the Dirac delta function $\delta(w)$, the inner integral over $w^j \in \mathcal{W}^i$ evaluates to 1 if $q^j(t^j) \in \mathcal{S}(w^i)$, and 0 otherwise. The outer integral over $w^i \in \mathcal{W}$ is equal to 1 only when $w^i = q^i(t^i)$. Therefore, the entire expression evaluates to 1 if $q^j(t^j) \in \mathcal{S}(q^i(t^i))$, and 0 otherwise.

### C. Sub-Period Formulation

Instead of considering the whole planning horizon $[0, T]$, sometimes it is useful to evaluate the connection probability within a sub-period of the planning horizon. Let $[t_0, t_f] \subseteq [0, T]$ denote a *sub-period* of the planning time horizon. Similar to Eq. (5), we can then define the connection probability within this sub-period $[t_0, t_f]$ as:

$$\begin{aligned}
&P_c(q^i, q^j; t_0, t_f) = \\
&\qquad \frac{1}{(t_f - t_0)^2} \int_{t_0}^{t_f} \int_{t_0}^{t_f} \gamma(q^i(t^i), q^j(t^j)) dt^j dt^i \quad (8)
\end{aligned}$$

As we will see later, to maintain connectivity over a sub-period $[t_0, t_f]$, we can either maximize Eq. (8) as an objective or enforce it to exceed a user-specified threshold as a constraint.

With this sub-period formulation, the intermittent connectivity requirement can be formulated as follows. We divide the time horizon $[0, T]$ into $N_p \in \mathbb{N}^+$ consecutive sub-periods, where each period $p \in I_p = \{1, \ldots, N_p\}$ is defined by its start and end time $\underline{t}_p, \bar{t}_p \in [0, T]$. Here, the adjacent sub-periods are consecutive, i.e., $\underline{t}_p = \bar{t}_{p-1}$. For each sub-period $p$, we constrain its connection probability to be greater than a user-defined threshold, thereby ensuring a minimum connection probability among robots over the entire time horizon. The relationship between the connection probability and the actual connection status among the robots is discussed in Sec. VII.

## V. Optimal Control and Optimality Conditions

### A. Problem Formulation

Using the ergodicity (2) and the sub-period connection probability (8), we formulate the multi-robot ergodic search with connection maintenance (MEC) problem as follows.

**Definition 3** (MEC Problem)**.**

$$\min_{x,u} \quad r_{\mathcal{E}}\mathcal{E}(\phi,q) + \int_0^T \frac{1}{2}u^T(t)R(t)u(t)dt \tag{9a}$$

$$\text{s.t.} \quad \dot{x} = f(x,u) \tag{9b}$$

$$x(0) = x_0 \tag{9c}$$

$$P_c(q^i,q^j;\underline{t}_p,\bar{t}_p) \geq \varepsilon_c, \forall (i,j)\in\mathcal{R}, \forall p \in I_p \tag{9d}$$

$$||q^i(t) - q^j(t)||_2 \geq \varepsilon_a, \forall (i,j)\in\mathcal{R}, \forall t \in [0,T] \tag{9e}$$

Here, the objective (9a) consists of the ergodicity of all robots and the control cost, with a hyper-parameter $r_{\mathcal{E}} \in \mathbb{R}^+$ defining the weight of the ergodicity, and a positive definite matrix $R(t) \in \mathbb{R}^{Nm\times Nm}, \forall t \in [0,T]$ defining the weight of the controls, respectively. The constraints (9b), (9c), (9d), and (9e) represent the constraints on the robot dynamics, initial state, sub-period connection probability, and collision avoidance, respectively, where $x_0 \in \mathcal{X}^N$ and $\varepsilon_c, \varepsilon_a \in \mathbb{R}^+$ are the initial state and constraint thresholds. Note that when the sub-period number $N_p = 1$, constraint (9d) is represented as $P_c(q^i,q^j;0,T) \geq \varepsilon_c$.

**Remark 1.** *In Eq. (9d), we impose a constraint on the connection probability for all pairs of robots, i.e., $\forall (i,j)\in\mathcal{R}$, to ensure strict pairwise connectivity. Furthermore, in some applications, this constraint can be modified to apply only to specific pairs of robots, as determined by a predefined connection graph topology [18, 23], e.g., $(i,j)\in\{(1,2)\}\subset\mathcal{R}$.*

### B. Optimality Conditions

To derive the first-order necessary (local) optimality condition for the MEC problem 3, we first define the Lagrange function. When the Lagrange function takes the standard Bolza form, the Pontryagin principle can be directly applied to obtain the optimality condition. However, there are two main challenges in the formulation of the Lagrange function:

- The ergodicity term $\mathcal{E}(\phi,q)$ in (9a) contains a quadratic term defined over the entire trajectories over the time horizon $[0,T]$ of all robots, rather than just at the terminal time, making it incompatible with the Bolza form. To address this, we can reformulate $\mathcal{E}(\phi,q)$ as a terminal term by introducing an auxiliary system state [7, 9, 30].
- The connection probability constraint (9d) is defined over each sub-period $p$ without a stage-wise form, making it incompatible with the stage cost structure of the Bolza form. This can be resolved by reformulating the connection probability constraint as stage-wise constraints by introducing the instantaneous connection probability.

With these reformulations, we can express the Lagrange function of MEC problem 3 in the Bolza form, allowing us to apply the Pontryagin principle to derive the first-order necessary conditions that characterize a locally optimal solution.

*1) Reformulation of Ergodicity:* By introducing an auxiliary system state, we can reformulate the ergodicity term in (9a) of the MEC problem into the following terminal form.

**Definition 4** (Terminal Form of Ergodicity)**.** *Let $s(t) = \big(s_{\mathbf{0}}(t), s_{(1,0,\cdots)}(t), \cdots, s_{\mathbf{k}_{|\mathcal{K}|}}(t)\big) \in \mathbb{R}^{|\mathcal{K}|}$ denote the* auxiliary system state *[7, 9, 30], where each element $s(t)$ is defined as $s_{\mathbf{k}}(t) = \frac{1}{N}\sum_{i\in I_N}\int_0^t F_{\mathbf{k}}(q^i(\tau))d\tau - t\phi_{\mathbf{k}}$, then the ergodicity (2) can be expressed as:*

$$\mathcal{E}(\phi,q) = \frac{1}{2}s^T(T)Q_{\mathcal{K}}s(T) \tag{10}$$

*with initial condition $s(0) = \mathbf{0}$ and the following differential constraints:*

$$\dot{s}(t) = g(x(t)) = \frac{1}{N}\sum_{i\in I_N} F(q^i(t)) - \Phi \tag{11}$$

Here, $Q_{\mathcal{K}} = \frac{2}{T^2}\operatorname{diag}(\Lambda_{\mathbf{0}}, \cdots, \Lambda_{\mathbf{k}_{|\mathcal{K}|}}) \in \mathbb{R}^{|\mathcal{K}|\times|\mathcal{K}|}$ represents a diagonal matrix constructed from the given elements. Additionally, $\Phi = \big(\phi_{\mathbf{0}}, \cdots, \phi_{\mathbf{k}_{|\mathcal{K}|}}\big)$ denotes the Fourier coefficient vector corresponding to the information distribution $\phi(w)$. Similarly, $F(w) = \big(F_{\mathbf{0}}(w), \cdots, F_{\mathbf{k}_{|\mathcal{K}|}}(w)\big)$ represents the vector of basis functions. Note that the summation $\sum_{i\in I_N}(\cdot)$ is evaluated component-wise across the elements of $F(w)$. To simplify the subsequent presentation, we introduce the notation $g(x(t))$ to represent the right-hand side expression of Eq. (11).

*2) Instantaneous Connection Probability:* For sub-period $p$, we evaluate the connection probability $P_c(q^i,q^j;\underline{t}_p,\bar{t}_p)$ by integrating the CIF (6) over the interval $[\underline{t}_p,\bar{t}_p]$, where the CIF is a function characterizing the robots' trajectories. At any time instant $t \in [\underline{t}_p,\bar{t}_p]$, the instantaneous connection probability can be formulated as follows[3].

$$P_c(q^i,q^j,t;\underline{t}_p,\bar{t}_p) = \frac{1}{(\bar{t}_p - \underline{t}_p)^2}\int_{\underline{t}_p}^{\bar{t}_p}\gamma(q^i(t),q^j(t^j))dt^j \tag{12}$$

To facilitate the construction of the Lagrange function, we can reformulate the connection probability constraint (9d) into an equivalent stage-wise form:

$$\int_{\underline{t}_p}^{\bar{t}_p} P_c(q^i,q^j,t;\underline{t}_p,\bar{t}_p) - \frac{\varepsilon_c}{\bar{t}_p - \underline{t}_p}dt \geq 0 \quad \forall (i,j)\in\mathcal{R}, \forall p \in I_p \tag{13}$$

*3) Lagrange Function:* The Lagrange function for the MEC problem 3 is formulated as:

$$\mathcal{L}(x,s,u,\rho_x,\rho_s,\rho_c,\rho_a) = \frac{r_{\mathcal{E}}}{2}s^T(T)Q_{\mathcal{K}}s(T) \tag{14}$$
$$+\int_0^T\Big\{l(x,u,t) + r_c\rho_c^T(t)c(x,u,t) + r_a\rho_a^T(t)a(x,u,t) +$$
$$\rho_x^T(t)(f(x(t),u(t)) - \dot{x}(t)) + \rho_s^T(t)(g(x(t)) - \dot{s}(t))\Big\}dt$$

where $\rho_x(t) \in \mathbb{R}^{Nn}, \rho_s(t) \in \mathbb{R}^{|\mathcal{K}|}, \rho_c(t) \in \mathbb{R}^{|\mathcal{R}|} \geq \mathbf{0}, \rho_a(t) \in \mathbb{R}^{|\mathcal{R}|} \geq \mathbf{0}$ are the Lagrange multipliers corresponding to

[3] If $t \notin [\underline{t}_p,\bar{t}_p]$, the instantaneous connection probability equals zero.

constraints (9b, 11, 9d, 9e), respectively. The coefficients $r_c, r_a \in \mathbb{R}^+$ are weight factors for constraints (9d, 9e). Note that $\rho_c(t)$ is piecewise constant over each sub-period, i.e., $\rho_c(t) = \rho_c^p \geq \mathbf{0}$ for $t \in [\underline{t}_p, \bar{t}_p], \forall p \in I_p$, because (9d) constrains the connection probability over each sub-period rather than at any specific time $t$. The component functions in the Lagrange function (14) are defined as:

$$
\begin{aligned}
l(x,u,t) &= \frac{1}{2}u(t)^T R(t) u(t) \qquad (15)\\
c(x,u,t) &= \left( -P_c(q^i, q^j, t; \underline{t}_p, \bar{t}_p) + \frac{\varepsilon_c}{\bar{t}_p - \underline{t}_p} \right)_{\forall (i,j) \in \mathcal{R}}\\
a(x,u,t) &= \left( -||q^i(t) - q^j(t)||_2 + \varepsilon_a \right)_{\forall (i,j) \in \mathcal{R}}
\end{aligned}
$$

where $l(x,u,t) \in \mathbb{R}$ denotes the stage cost, $c(x,u,t) \in \mathbb{R}^{|\mathcal{R}|}$ denotes the stage-wise connection probability constraints vector for (9d) over any sub-period $p$ in which time $t$ lies, and $a(x,u,t) \in \mathbb{R}^{|\mathcal{R}|}$ represents the collision avoidance constraints vector for (9e), all evaluated at time $t \in [0,T]$. For brevity, we define $\mu(t) = (\rho_c(t), \rho_a(t))$ and $\mathcal{I}(x,u,t) = (r_c c(x,u,t), r_a a(x,u,t))$ (or simply $\mathcal{I}(t)$) as the concatenated vectors of multipliers and inequality constraints, respectively.

*4) Hamiltonian:* Based on the Lagrange function (14), the Hamiltonian of the MEC problem at time $t$ is defined as:

$$
\begin{aligned}
H(x,s,u,\rho_x,\rho_s,\mu,t) = l(x,u,t) + \mu^T(t)\mathcal{I}(x,u,t) + \\
\rho_x^T(t) f(x(t),u(t)) + \rho_s^T(t) g(x(t)) \qquad (16)
\end{aligned}
$$

**Theorem 2** (Necessary Optimality Condition)**.** *For a locally optimal control law $u$ and the resulting state trajectory $x$, the following conditions must be satisfied:*

$$
\begin{aligned}
\dot{x} &= \nabla_{\rho_x} H = f(x,u) \text{ with } x(0) = x_0 \qquad (17a)\\
\dot{s} &= \nabla_{\rho_s} H = g(x) \text{ with } s(0) = \mathbf{0} \qquad (17b)\\
-\dot{\rho_x} &= \nabla_x H \qquad (17c)\\
\rho_x(T) &= \mathbf{0}\\
-\dot{\rho_s} &= \nabla_s H = \mathbf{0} \qquad (17d)\\
\rho_s(T) &= \left. \frac{\partial \left( \frac{r_\mathcal{E}}{2} s^T(T) Q_\mathcal{K} s(T) \right)^T}{\partial s} \right|_{s(T)} = r_\mathcal{E} Q_\mathcal{K} s(T)\\
\nabla_\mu H &= \mathbf{0} \qquad (17e)\\
u^*(t) &= \underset{u(t) \in \mathcal{U}^N}{\arg\min}\, H(\cdots, t),\ t \in [0,T] \qquad (17f)
\end{aligned}
$$

*Proof.* Pontryagin's minimum principle [36] provides the necessary conditions for a trajectory to be optimal, which consist of the state equations with initial conditions (Eq. (17a) for $x$ and Eq. (17b) for $s$), the costate equations with terminal conditions (Eq. (17c) for $x$ and Eq. (17d) for $s$), and the inequality multiplier equation Eq. (17e). The optimal control input can be obtained by minimizing the Hamiltonian (16) within the control space $\mathcal{U}^N$, which yields Eq. (17f). The proof is provided in Appendix A-B. □

## VI. Numerical Approach

The robot dynamics (9b) and inequality constraints $\mathcal{I}(t)$ introduce nonlinearity into the optimization problem. While the optimality condition (17) provides a theoretical foundation, directly solving for the optimal control law remains computationally challenging. Therefore, we propose iterative-MEC (IMEC), an iterative optimization approach that numerically solves the MEC problem 3 based on the derivation of (17).

IMEC first converts the MEC problem to the form consisting of the augmented cost and robot dynamics constraint using the augmented Lagrangian method (ALM) in Sec. VI-A [37, 38]. Second, IMEC follows the idea of iterative LQR (iLQR) to linearize the cost and dynamics to define a sub-problem in each iteration (Sec. VI-B), and iteratively solves the sub-problem using the Linear Quadratic Regulator (LQR) for trajectory optimization [8, 38] (Sec. VI-C). Additionally, a technique to avoid gradient vanishing is introduced in Sec. VI-D.

### A. Augmented Lagrangian Problem

*1) Augmented Cost:* In Sec. V-B4, we formulate the Hamiltonian (16) based on the Lagrange function (14). The optimal control law is obtained by minimizing the Hamiltonian as in (17f). To improve convergence and handle inequality constraints more robustly, in addition to the corresponding multiplier terms in Eq. (14), we add a penalty term for inequality constraints following the ALM [37, 38]. Let $l_\mathcal{I}(x,u,t)$, with penalty coefficient $r \in \mathbb{R}^+$, denote the augmented term at time $t$ containing the multipliers and penalty terms for the integral and stage-wise constraints (9d) and (9e). Besides, based on the constraint violation, the multiplier $\mu(t) = (\rho_c(t), \rho_a(t))$ can be updated in each iteration using [37, 38]:

$$
\begin{aligned}
\rho_c^p &\leftarrow \max\left\{ \mathbf{0}, \rho_c^p + r \cdot \int_{\underline{t}_p}^{\bar{t}_p} r_c c(x,u,t) dt \right\} \qquad (18a)\\
\rho_a(t) &\leftarrow \max\left\{ \mathbf{0}, \rho_a(t) + r \cdot r_a a(x,u,t) \right\} \qquad (18b)
\end{aligned}
$$

During optimization, constraints $\mathcal{I}(t), t \in [0,T]$ are incorporated into the cost (optimization objective). Therefore, the augmented MEC problem is formulated as:

$$
\begin{aligned}
&\min_{x,u} J(x,u) \quad \text{s.t. } (9b), (9c) \text{ where} \qquad (19a)\\
&J(x,u) = r_\mathcal{E} \mathcal{E}(\phi, q) + \int_0^T l(x,u,t) + l_\mathcal{I}(x,u,t) dt \qquad (19b)
\end{aligned}
$$

### B. Linearization

*1) Dynamics Linearization:* Let $\bar{x}(t), \bar{u}(t), t \in [0,T]$ denote the linearized trajectory. The linearized robot dynamics about Eq. (9b) is formulated as follows:

$$
\begin{aligned}
&\dot{\delta x}(t) = A(t)\delta x(t) + B(t)\delta u(t) \text{ with} \qquad (20)\\
&A(t) = \left. \frac{\partial f(x,u)}{\partial x} \right|_{(\bar{x}(t), \bar{u}(t))},\ B(t) = \left. \frac{\partial f(x,u)}{\partial u} \right|_{(\bar{x}(t), \bar{u}(t))}
\end{aligned}
$$

where $\delta x(t) = x(t) - \bar{x}(t)$ and $\delta u(t) = u(t) - \bar{u}(t)$ denote the state and control deviations with respect to $\bar{x}(t)$ and $\bar{u}(t)$, respectively. Here, $A(t)$ and $B(t)$ represent the corresponding state and control matrices.

*2) Cost Linearization:* We aim to determine appropriate deviations $\delta x$ and $\delta u$ that ensure the cost (19b) decreases. Specifically, given the linearization trajectory $\bar{x}, \bar{u}$, the optimization objective is defined as (ignoring higher-order terms):

$$\begin{aligned}\Delta\mathcal{J}(\delta x, \delta u) &= J(\bar{x}+\delta x, \bar{u}+\delta u) - J(\bar{x}, \bar{u}) \\ &\approx \left.\frac{\partial J}{\partial x}\right|_{(\bar{x},\bar{u})} \delta x + \left.\frac{\partial J}{\partial u}\right|_{(\bar{x},\bar{u})} \delta u \end{aligned} \tag{21}$$

The corresponding terms are formulated as follows:

$$\frac{\partial J}{\partial x} = r_{\mathcal{E}} \frac{\partial \mathcal{E}}{\partial x} + \int_0^T \frac{\partial l(x,u,t) + \partial l_{\mathcal{I}}(x,u,t)}{\partial x} dt \tag{22}$$

$$\begin{aligned} &= r_{\mathcal{E}} \frac{\partial \mathcal{E}}{\partial s}\frac{\partial s}{\partial x} + \int_0^T l_x(t) + l_{\mathcal{I}x}(t) dt \\ &= r_{\mathcal{E}} s^T(T) Q_{\mathcal{K}} \int_0^T \frac{1}{N}\sum_{i\in I_N} \frac{\partial F(q^i(t))}{\partial x} dt \\ &\quad + \int_0^T l_x(t) + l_{\mathcal{I}x}(t) dt \\ &= \int_0^T \underbrace{r_{\mathcal{E}} \frac{s^T(T) Q_{\mathcal{K}}}{N} \sum_{i\in I_N} \frac{\partial F(q^i(t))}{\partial x} + l_x(t) + l_{\mathcal{I}x}(t)}_{\alpha^T(t)} \, dt \end{aligned} \tag{23}$$

and

$$\frac{\partial J}{\partial u} = \int_0^T l_u(t) + l_{\mathcal{I}u}(t) dt = \int_0^T \underbrace{u^T(t) R(t)}_{\beta^T(t)} dt \tag{24}$$

Note that $Q_{\mathcal{K}}$ is a symmetric matrix, i.e., $Q_{\mathcal{K}}^T = Q_{\mathcal{K}}$.

With the introduced variables $\alpha(t)$ and $\beta(t)$ in Eq. (22, 24), the optimization objective in (21) can be reformulated as:

$$\Delta\mathcal{J}(\delta x, \delta u) \approx \int_0^T \alpha^T(t)\delta x(t) + \beta^T(t)\delta u(t) dt \tag{25}$$

### C. Iterative Optimization

*1) Define the LQR Problem:* Given the state and control trajectories $\bar{x}$ and $\bar{u}$, we can derive the linear formulation of the objective (21) and linear robot dynamics (20). In each iteration, we solve the following optimal control problem:

$$\min_{\delta x, \delta u} \Delta\mathcal{J}(\delta x, \delta u) \tag{26a}$$

$$+ \int_0^T \frac{1}{2}\delta x^T(t) Q_\delta(t) \delta x(t) + \frac{1}{2}\delta u^T(t) R_\delta(t) \delta u(t) dt$$

$$\text{s.t.} \quad \dot{\delta x}(t) = A(t)\delta x(t) + B(t)\delta u(t) \tag{26b}$$

$$\delta x(0) = x_0 - \bar{x}(0) = \mathbf{0} \tag{26c}$$

where objective (26a) contains both linear and quadratic terms with cost matrices $Q_\delta(t) \in \mathbb{R}^{Nn\times Nn}, R_\delta(t) \in \mathbb{R}^{Nm\times Nm}$. Eq. (26b) represents the linearized dynamics, and Eq. (26c) ensures the state trajectory starts from $x_0$, satisfying initial condition (9c). This is a typical optimal control problem that can be solved using Linear Quadratic Regulator (LQR) [39].

**Algorithm 1** Iterative-MEC

1: Initialize: Linearization trajectory $\bar{x}, \bar{u}$, multiplier $\mu(t)$. Refer to Tab. I for other parameters.
2: **for** $k = 1$ to $k_m$ **do**
3: $\quad \delta u \leftarrow$ Using LQR to solve Problem (26) with initial guess $\delta x = \mathbf{0}$, $\delta u = \mathbf{0}$
4: $\quad$ Using line search to get the ideal step size $\theta^\star$
5: $\quad u \leftarrow \bar{u} + \theta^\star \delta u$ ▷ Update control trajectory
6: $\quad x \leftarrow$ forward roll-out with control $u$ under dynamics
7: $\quad$ **if** $J(\bar{x}, \bar{u}) - J(x, u) \geq \varepsilon_\mu$ **then** ▷ $\varepsilon_\mu \in \mathbb{R}^+$
8: $\quad\quad$ Update the multiplier $\mu(t)$ ▷ See (18)
9: $\quad$ **else**
10: $\quad\quad$ Increase the penalty $r = \hat{\alpha}_r \cdot r$ ▷ $\hat{\alpha}_r > 1$
11: $\quad\quad$ Decrease $\varepsilon_\mu = \hat{\alpha}_\mu \cdot \varepsilon_\mu$ ▷ $1 > \hat{\alpha}_\mu > 0$
12: $\quad$ **if** Meet the termination criteria **then**
13: $\quad\quad$ Return state and control trajectory $x, u$
14: $\quad \bar{x}, \bar{u} \leftarrow x, u$ ▷ Update linearized trajectory

*2) Iterative Solving Approach:* Alg. 1 outlines the iterative solving approach. First, we initialize the multiplier using Eq. (18) to identify active constraints in $\mathcal{I}(t), t \in [0, T]$ (Line 1). Note that the linearization trajectory $\bar{x}$ is derived from the roll-out process based on the given initial control trajectory $\bar{u}$ and the initial state $x_0$. Then, based on current trajectories $\bar{x}, \bar{u}$, we linearize Problem (19) and apply LQR to solve Problem (26), obtaining control deviations $\delta u$ (Line 3). Next, we employ line search to find a control $u$ that decreases the objective (19b) (Lines 4-5). The multiplier or penalty coefficient is updated based on the convergence conditions (Lines 7-11). Finally, we return the state and control trajectories $x$ and $u$ when the termination criteria are satisfied. Otherwise, the current state and control $\bar{x}, \bar{u}$ are updated (Line 14). In this paper, the termination criteria are defined as $|J(\bar{x}, \bar{u}) - J(x, u)| \leq 10^{-6}$ and the sum of inequality violations is less than $0.01$.

### D. Approximation for CIF

In Eq. (22), there exists a term $l_{\mathcal{I}_x}(t)$ containing the partial derivative of the CIF (6) with respect to the state $x$. However, this function lacks smooth derivatives, which challenges the trajectory optimization approach. A possible solution is to approximate the CIF to obtain smooth derivatives. Let $\Gamma(\cdot,\cdot)$ denote the approximated CIF. In this paper, the connection area is represented as a sphere (or circle) centered at $w^i$ with connection range $R_c$ for robot $i$, formally defined as $\mathcal{S}(w^i) := ||w - w^i||_2 \leq R_c, w \in \mathcal{W}$. We consider two approximated CIFs, and their performance is discussed in Sec. VII-B3.

- Gaussian CIF:

$$\Gamma(w^i, w^j) = \exp\left(-\frac{||w^j - w^i||_2^2}{r_\Gamma \cdot 2R_c^2}\right) \tag{27}$$

- Sigmoid CIF:

$$\Gamma(w^i, w^j) = \frac{1}{1 + \exp\left(r_\Gamma\left(\frac{||w^j - w^i||_2^2}{R_c^2} - 1\right)\right)} \tag{28}$$

Here, $r_\Gamma > 0$ is a hyper-parameter related to the magnitude of the gradient. For higher $r_\Gamma$, the Sigmoid CIF (28) provides steeper gradients than the Gaussian CIF (27) near $||w^j - w^i||_2 = R_c$. Therefore, the Sigmoid CIF can potentially better represent the relationship between connection probability and inter-robot distances. Besides, while the Gaussian CIF provides a coarse approximation, it offers smoother gradients, which can be important for nonlinear optimization in practice. Finally, the approximated CIF's shape can be adjusted via the parameter $r_\Gamma$, which is set to 1 for all CIFs in this paper.

## VII. Experimental Results

This section seeks to answer the following three categories of questions. First, we examine the effect of the probabilistic connectivity measure on the optimized trajectories over a finite time horizon $[0, T]$ in practice. Specifically, we address the following questions:

- Sec. VII-B1: How does increased connection probability correlate with the actual connection time over $[0, T]$?
- Sec. VII-B2: To what extent does maintaining higher connection probability affect the information searching performance measured by ergodicity?
- Sec. VII-B3: How different approximated CIFs $\Gamma(\cdot, \cdot)$ (as discussed in Sec. VI-D) perform in practice?

Second, we explore how various hyper-parameters in the MEC problem and our planning algorithm influence the resulting trajectories. Specifically, we investigate:

- Sec. VII-C: What are the benefits of the sub-period formulation, and how does the sub-period number affect the optimized trajectories?
- Sec. VII-D: How does the horizon $T$ influence the actual connectivity, the robots' trajectories, and the resulting spatial distributions?
- Sec. VII-B, VII-C, VII-E: How does our method perform in different information maps?

Third, we evaluate our method (using probabilistic connection) in comparison to baseline approaches to understand how different algorithms balance between ergodic search and connectivity maintenance. Specifically, we investigate:

- Sec. VII-E: How does our probabilistic connectivity maintenance approach compare to a method that encourages all robots to stay connected at all times?
- Sec: VII-F: What are the pros and cons of probabilistic connection versus several existing connectivity maintenance strategies: enforcing periodic connectivity, enforcing strict all-time connectivity, and no connectivity requirement during the ergodic search?

Finally, we evaluate the scalability of our approach with increasing numbers of robots in Sec. VII-G.

### A. Experiment Settings

*1) Parameters:* In our experiments, each robot $i$ has the state $x^i(t) = (q^i(t), v^i(t))$ and control input (acceleration or force) $u^i(t) = (u_1^i(t), u_2^i(t))$, where $q^i(t)$ and $v^i(t)$ denote the robot's position and velocity in the workspace, respectively. The robot dynamics is described as a double integrator model: $\dot{x}^i = (\dot{q}^i, \dot{v}^i) = (v^i, u^i)$. For robot $i$, the initial guess for the control trajectory $u^i$ is set to zero input, i.e., $u^i = \mathbf{0}$. Given the initial state $x_0^i$, the resulting state trajectory can then be determined by forward simulation (i.e., rollout). All other experimental parameters are summarized in Tab. I. Unless explicitly stated otherwise, these parameters remain consistent throughout all experiments.

*2) Performance Indicators:* In this section, we introduce several indicators to evaluate the experimental results.

- *Ergodicity* $\mathcal{E}$: Lower ergodicity means better information gathering performance (Eq. (2)).
- *Average Connection Ratio* $\bar{R}_c$: $\bar{R}_c$ measures the proportion of time that robots are connected throughout the entire time horizon $T$, which is calculated by:

$$\bar{R}_c = \mathbb{E}_{(i,j)\in\mathcal{R}} \left\{ \mathbb{E}_{t\in[0,T]} \left\{ \mathbf{1}(||q^i(t) - q^j(t)||_2 \leq R_c) \right\} \right\}$$

  where $\mathbb{E}$ denotes the average operator and $\mathbf{1}(\cdot)$ is an indicator function that returns 1 if the condition is true and 0 otherwise.
- *Average Connection Probability* $\bar{P}_c$: $\bar{P}_c$ is the average connection probability (8) over all sub-periods.

$$\bar{P}_c = \mathbb{E}_{(i,j)\in\mathcal{R}} \left\{ \mathbb{E}_{p\in I_p} \left\{ P_c(q^i, q^j; \underline{t}_p, \bar{t}_p) \right\} \right\}$$

### B. Connection Probability

This section discusses the relationship between average connection probability $\bar{P}_c$ and two performance indicators: average connection time $\bar{R}_c$ (shown in blue) and ergodicity $\mathcal{E}$ (shown in orange), as illustrated in Fig. 3. This test is conducted across different information maps $\phi(w)$ (denoted as Map 1-3) and employs both the Sigmoid and Gaussian CIF. The additional experimental parameters are: robot number $N = 4$, simulation steps $N_T = 300$, and sub-period number

TABLE I
Experiment Parameters

| Symbols | Value / Range | Description |
|---|---|---|
| $\mathcal{W}$ | $[0, 3] \times [0, 2.5]$ m | Workspace |
| $\mathcal{K}$ | $[0, \cdots, 10] \times [0, \cdots, 10]$ | Frequency set |
| $\Delta t, T$ | 0.1 s, $N_T\,\Delta t$ s | Time step, horizon |
| $R(t)$ | $\mathrm{diag}(5, 5, \cdots) \times 10^{-3}$ | |
| $Q_\delta(t)$ | $\mathrm{diag}(.1, .1, 1, 1, \cdots) \times 10^{-3}$ | Cost matrix |
| $R_\delta(t)$ | $\mathrm{diag}(5, 5, \cdots) \times 10^{-3}$ | |
| $r_\mathcal{E}, r_c, r_a$ | $1.0, 0.1/\varepsilon_c, 0.1/(\varepsilon_a\lvert\mathcal{R}\rvert)$ | Cost coefficient |
| $x_0$ | / | Initial state |
| $u$ | $[-\mathbf{0.5}, \mathbf{0.5}]$ m/s$^2$ | Control saturation |
| $R_c$ | 0.5m | Connection range |
| $\varepsilon_a$ | 0.3 m | Avoidance limit (9e) |
| $\varepsilon_c$ | / | Measure limit (9d) |
| $N$ | / | Robot number |
| $N_T$ | / | Simulation steps |
| $N_p$ | / | Sub-Period number |
| $\mu(t), k_m$ | $\mathbf{0}, 2000$ | |
| $r, \hat{\alpha}_r$ | $1.0, 1.05$ | Parameters in Alg. 1 |
| $\varepsilon_\mu, \hat{\alpha}_\mu$ | $0.1, 0.95$ | |

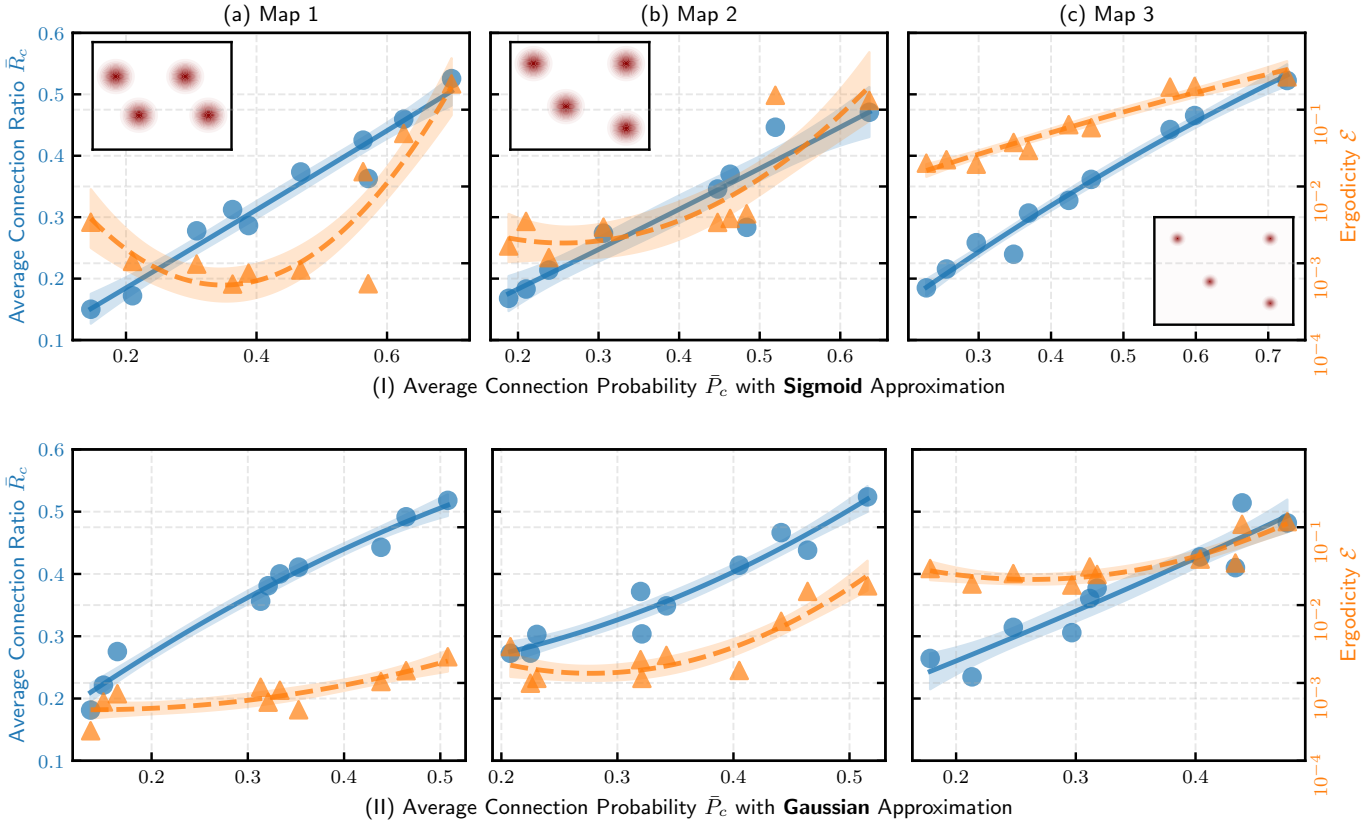


Fig. 3. The relationship between average connection probability $\bar{P}_c$ (the horizontal axis) and two metrics (the left and right vertical axes): average connection time ratio $\bar{R}_c$ (blue data) and ergodicity $\mathcal{E}$ (orange data). The subfigure (I) uses the Sigmoid CIF, while the subfigure (II) uses the Gaussian CIF. Each column corresponds to the same information distribution maps $\phi(w)$, denoted as Map 1,2, and 3.

$N_p = 3$. The connection probability threshold in Eq (9d) is set as $\varepsilon_c \in [0.05, 0.5]$ with a step size of 0.05.

*1) Connection Probability over Connection Ratio:* As shown by the blue data points in Fig. 3-(I, II), the experimental results reveal a positive correlation between the average connection ratio $\bar{R}_c$ and average connection probability $\bar{P}_c$ among the test instances. This correlation suggests that higher connection probabilities tend to result in increased actual connection time ratios between the robots. However, it is noted that the blue dots in Fig. 3-(I, II) do not lie perfectly on the same straight line, indicating that a higher $\bar{P}_c$ does not always correspond to a higher $\bar{R}_c$. This is not a surprise due to the inherent probabilistic nature of the connection probability.

*2) Connection Probability over Ergodicity:* As shown by the orange data points in Fig. 3-(I, II), the ergodicity $\mathcal{E}$ increases (i.e., worsens) as the average connection probability $\bar{P}_c$ rises for most test instances. The reason is that with a higher connection probability $\bar{P}_c$, the robots need to gather together more frequently to establish the connection, which prevents the robots from covering a widespread information distribution and thus lowers the ergodicity.

*3) CIF Approximation Methods Comparison:* Comparing subfigures (I) and (II) in Fig. 3, we observe that the Gaussian CIF demonstrates slightly better (lower) ergodicity $\mathcal{E}$ and corresponds to a similar average connection time $\bar{P}_c$. This observation aligns with the discussions in Sec. VI-D[4].

### C. Sub-Period Experiments

*1) Varying Sub-Period Numbers:* In this sub-section, the connection probability threshold is set to $\varepsilon_c = 0.2$. The sub-period number $N_p$ takes values from the set $N_p \in \{1, 2, 3, 4, 5, 6\}$

As shown in Fig. 4, as the sub-period number $N_p$ increases, the average connection probability $\bar{P}_c$ generally increases (subfigure (a)), the average connection ratio $\bar{R}_c$ increases (subfigure (b)), and the ergodicity rises (subfigure (c)). A possible reason is that, with a higher number of sub-periods, the robots have to maintain a certain level of connection probability in each sub-period. It makes the robots gather together more frequently (i.e., $\bar{P}_c$ and $\bar{R}_c$ rise), which, in turn, prevents the robots from ergodically covering the information map (i.e., $\mathcal{E}$ increases).

*2) Impact of Sub-Period Formulation:* In this sub-section, we set the number of robots to $N = 2$ and the connection probability threshold to $\varepsilon_c = 0.2$. We compare the scenarios of $N_p = 1$ (with only one period) and $N_p = 3$.

[4]In the following experiments, unless otherwise stated, the information distribution is set to Map 1 under the fixed simulation steps $N_T = 300$, and the Gaussian CIF is used.

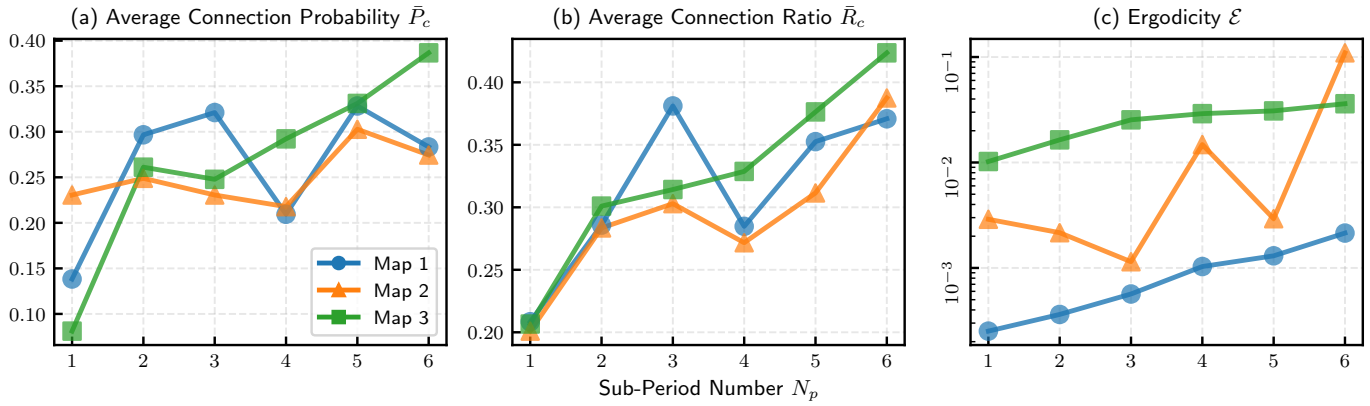


Fig. 4. Illustration of the impact of varying sub-period numbers on the following performance indicators (a): average connection probability $\bar{P}_c$, (b): average connection ratio $\bar{R}_c$, (c): ergodicity $\mathcal{E}$.

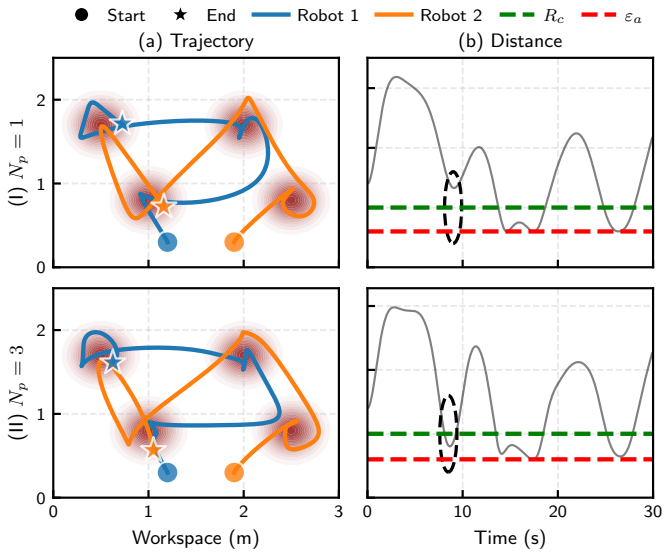


Fig. 5. Comparison of robot trajectories and inter-robot distances for sub-period numbers $N_p \in \{1, 3\}$. (a): Robot trajectories, (b): Inter-robot distance over time, where $R_c$ and $\varepsilon_a$ denote the connection range and the collision avoidance threshold.

As shown in Fig. 5-(I)-(b), when the connection probability is constrained to be greater than $\varepsilon_c$ over the entire time horizon $[0, T]$ ($N_p = 1$), the robot pairs lose connection during the time range $[0, 10]$ s, as the distance exceeds the connection range $R_c$. In contrast, as shown in subfigure (II)-(b), with $N_p = 3$, the robots establish the connection when each sub-period's connection probability is constrained to be greater than $\varepsilon_c$. The reason is that the sub-period formulation divides the time horizon into intervals of shorter length. Unlike planning with the entire horizon $[0, T]$, which only considers the spatial distribution over the entire horizon without considering meeting "at the same time", these shorter intervals are more likely to make the robots reach certain locations "at the same time" and thus achieve better connectivity. This approach ensures connectivity within each sub-period, preventing long disconnections.

Combined with the results in the previous sub-section, there is a trade-off between ergodicity and connectivity: planning with a large number of sub-periods tends to encourage better connectivity and worse ergodicity, while having a smaller number of sub-periods tends to encourage better ergodicity and worse connectivity.

### D. Planning Horizon

In this section, the parameters remain consistent with those in Sec. VII-C2 ($N = 2$, $N_p = 1$, $\varepsilon_c = 0.2$), and we fix the sub-period number $N_p = 1$ to study the impact of simulation steps $N_T$, which takes values $N_T \in \{100, 200, 300, 400\}$.

As shown in Fig. 6, as the horizon increases, the trajectory heatmaps of the two robots increasingly align with the information map, resulting in a decrease in ergodicity (as indicated by the orange data points in Fig. 7). This observation is consistent with the definition of ergodic search. Notably, the trajectories of the two robots do not merely search specific (partial) peaks of the information distribution; rather, both trajectories continuously encompass all peaks. This reflects the role of the connection probability $P_c$, as we aim for the robots to accomplish both the ergodic search task and maintain probabilistic connectivity.

In the meanwhile, as shown in Fig. 7, the average connection time ratio $\bar{R}_c$ decreases as $N_T$ increases. Compared with Fig. 6-(IV), although the frequencies of the robots gathering together at the same location increase, the robots go to the same location at different times, which leads to a decreasing $\bar{R}_c$. This indicates that as the horizon lengthens, achieving the same level of connection probability becomes easier while minimizing ergodicity. For example, this can be achieved through rapid movement among information peaks, resulting in the phenomenon of "meeting at the same location at different times".

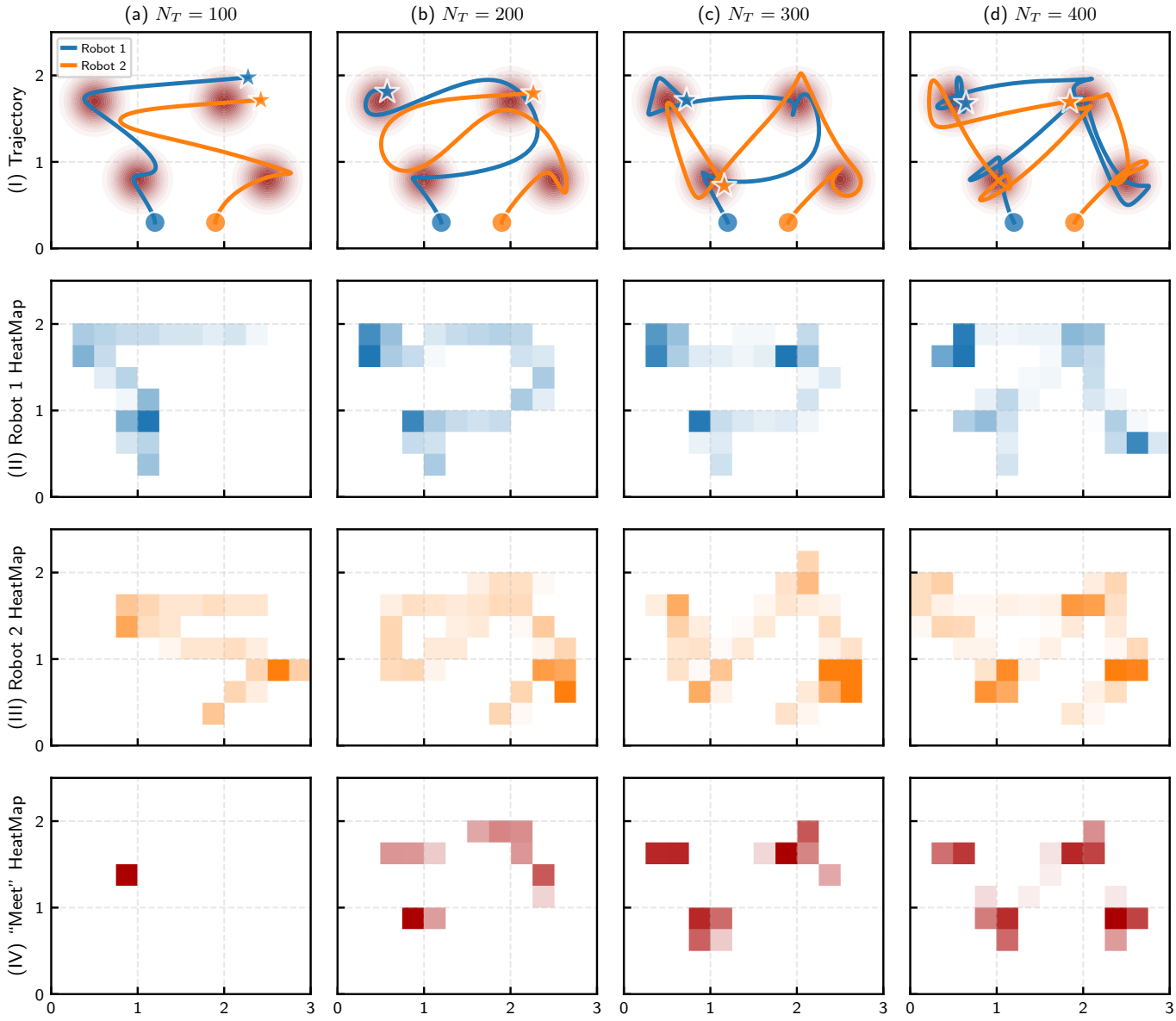


Fig. 6. The trajectories of two robots are illustrated in the first row (I), together with their corresponding heatmaps in the second (II) and third row (III). The fourth row (IV) presents a heatmap depicting the regions visited by both robots throughout the entire planning horizon $[0, T]$.

### *E. Comparison with a Variant Approach*

The definition of the connection probability (8) involves a double integral of $\gamma(q^i(t^i), q^j(t^j))$ over time, where the integrated variable $q$ is associated with different time variables $t^i$ and $t^j$. For comparison, by considering trajectories $q$ at the same time variable, we can define the following variant:

$$\tilde{P}_c(q^i, q^j; t_0, t_f) = \frac{1}{t_f - t_0} \int_{t_0}^{t_f} \gamma(q^i(t), q^j(t)) dt \qquad (29)$$

Here, $\tilde{P}_c$ calculates the ratio of two robots' connection time within the interval $[t_0, t_f]$. Note that, since both $q^i$ and $q^j$ are related to the same time variable $t$, $\tilde{P}_c$ corresponds to the case where the two robots $i, j$ reach certain locations "at the same time", which differs from $P_c$ in Eq. (8) that considers the spatial distribution over the entire horizon.

With $\tilde{P}_c$, we introduce a variant approach: we substitute $\tilde{P}_c$ for $P_c$ in Eq. (9d) of the MEC problem 3. The Gaussian CIF (27) is used to approximate $\tilde{P}_c$ for optimization. We also use Alg. 1 to solve the variant problem. Intuitively, this variant approach encourages all robots to stay connected at all times over each sub-period in a soft manner by considering the variant connectivity constraint $\tilde{P}_c$.

In this section, all parameters remain consistent with those outlined in Sec. VII-B. As shown in Fig. 8, the experimental results obtained using probabilistic connectivity as defined in Eq. (8) achieve better ergodicity than this variant approach

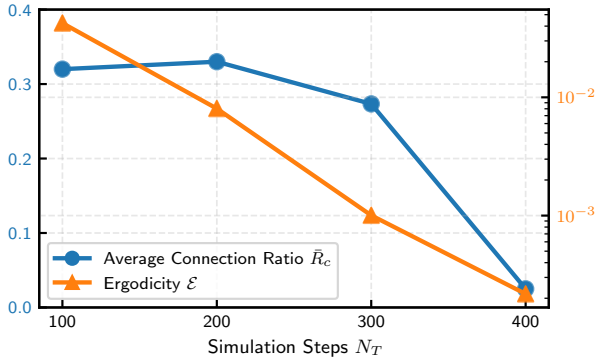


Fig. 7. The relationship between the number of simulation steps $N_T$ and two performance indicators: the average connection ratio $\bar{R}_c$ (blue) and ergodicity $\mathcal{E}$ (orange).

(about 0.65 times). Specifically, for ergodicity $\mathcal{E}$, the blue data points exhibit lower values. This demonstrates that probabilistic connectivity provides greater flexibility in optimizing the trajectories of the robots, while this variant approach encourages all robots to stay connected at all times, which can lead to poor ergodicity.

### F. Comparison with Other Connection Policies

In this section, we set the parameters to $N = 4$, $N_T = 300$, and $N_p = 3$, consistent with Sec. VII-B. We compare the results obtained under different connection policies. Additionally, we consider obstacles modeled as circles, defined by their radius and center, denoted as $O_R$ and $O_C$, respectively, as illustrated in Fig. 9. Note that in practice, robots have a physical volume, and we represent obstacles as inflated circles surrounding the actual obstacle. The corresponding collision avoidance constraint for the obstacles is defined as follows:

$$||q^i(t) - O_C||_2 \geq O_R, \forall t \in [0, T], \forall i \in I_N \tag{30}$$

In this experiment, we consider two obstacles modeled by their centers located at $O_C = (1.1, 1.5)$ m and $O_C = (1.9, 1.0)$ m, with each obstacle having a radius of $O_R = 0.2$ m. Here, our IMEC considers the additional collision avoidance constraint (30) with a threshold of $\varepsilon_c = 0.25$.

*1) Against Baseline with Periodic Connection:* We use the concept of periodic connection in [17], and introduce a baseline method that requires each pair of robots to gather together at the end of each sub-period, specifically at times $10, 20, 30$ s in our tests. The connection location selection is to be determined by the planner. Specifically, this baseline method solves the following optimization problem:

$$\text{Problem 3 without } (9d) \tag{31a}$$

$$\text{s.t.} \quad ||q^i(\bar{t}_p) - q^j(\bar{t}_p)||_2 \leq R_c, \forall p \in I_p, (i,j) \in \mathcal{R} \tag{31b}$$

$$(30)$$

As shown in Fig. 9, both methods satisfy the condition of "achieving connection in each sub-period" (as shown in subfigure (d)). The ergodicity achieved by our method is $\mathcal{E} = 0.001987$, while the baseline yields $\mathcal{E} = 0.009762$, which is about 4x higher than our method. It shows the advantages of probabilistic connectivity, as it allows the planner to select connection locations and time more flexibly by only enforcing a certain probability on establishing the inter-robot connection.

TABLE II
COMPARISON WITH STRICT ALL-TIME AND NO CONNECTIVITY

| | Ergodicity $\mathcal{E}$ (Lower is better) | Avg. connection ratio $\bar{R}_c$ (Higher is better) | Robots connected in all sub-periods? |
|---|---|---|---|
| B1 | $9.1 \times 10^{-3}$ | **0.70** | False |
| B2 | $9.5 \times 10^{-5}$ | 0.21 | False |
| Ours | $\mathbf{2.0 \times 10^{-3}}$ | 0.29 | **True** |

*2) Against Baselines with Strict All-Time Connectivity and Without Connectivity:* Here we ran experiments with two additional baselines: (B1) enforcing strict all-time connectivity constraints during planning, and (B2) omitting connectivity constraints entirely (i.e., robots only execute ergodic search). All other experimental settings are consistent with those described in Sec. VII-F. The corresponding results are presented in Tab. II. B1 achieves the worst ergodic search performance and the highest $\bar{R}_c$. In contrast, B2 achieves much better (smaller) ergodicity at the cost of poor connectivity. Compared with B1 and B2, our IMEC achieves moderate ergodicity while maintaining connectivity among all robot pairs in all sub-periods. It validates the adaptability of our proposed probabilistic measure, which balances ergodicity with connectivity maintenance. Note that B1 imposes many constraints, which frequently leads to convergence to infeasible local minima where some constraints are unsatisfied.

### G. Scalability

To evaluate scalability, we tested 5 to 10 robots in a $[0, 10] \times [0, 10]$ m workspace over a 100 s horizon ($\Delta t = 1$ s) using a Gazebo-based simulator, Crazysim [40]. The information distribution map is set to Map 1, as shown in Fig. 3-(I)-(a). Our planner terminates when the sum of all constraint violations falls below a threshold of 0.01. The runtimes for 5 to 10 robots are $\{26.4, 36.4, 64.1, 102.3, 214.5, 221.9\}$ s, respectively, on a laptop (Intel i7-12700H). We observe that, as the number of robots increases, the runtime also increases. A possible reason is that inter-robot collision avoidance becomes more challenging. Decentralized computation and real-time control are needed to handle significantly larger robot teams.

### H. Hardware Experiment

The hardware experiment is conducted following the results using our IMEC presented in Sec. VII-F, using the Crazyflie 2.1 [41], Crazyswarm2 [42], ROS2 [43], and a motion capture system. Each Crazyflie employs PID-based position control to resist the effects of unmodeled dynamics and motion disturbances. As shown in Fig. 10, the drones executed the optimized trajectories, built connections intermittently, avoided inter-agent collision and static obstacles, and searched the information map ergodically. This experiment validates that our IMEC can be applied to real robots in a lab setting.

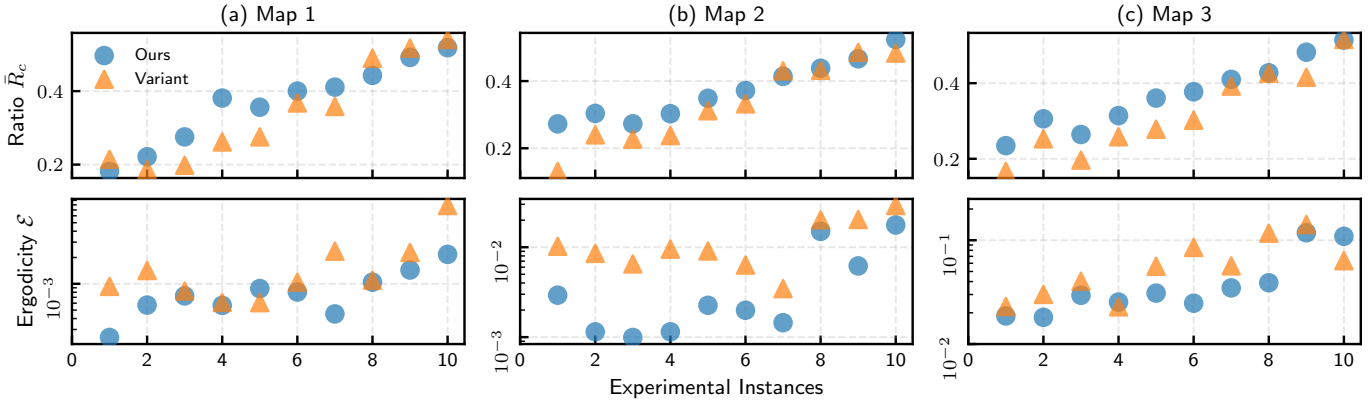


Fig. 8. Comparison of the performance of probabilistic connectivity (blue data point) as defined in Eq. (8) and variant connectivity (orange data point) as described in Eq. (29) across varying testing instances. The horizontal axis is the index of test instances, and the vertical axes are the average connection ratio $\bar{R}_c$ (upper figure) and ergodicity $\mathcal{E}$ (lower figure).

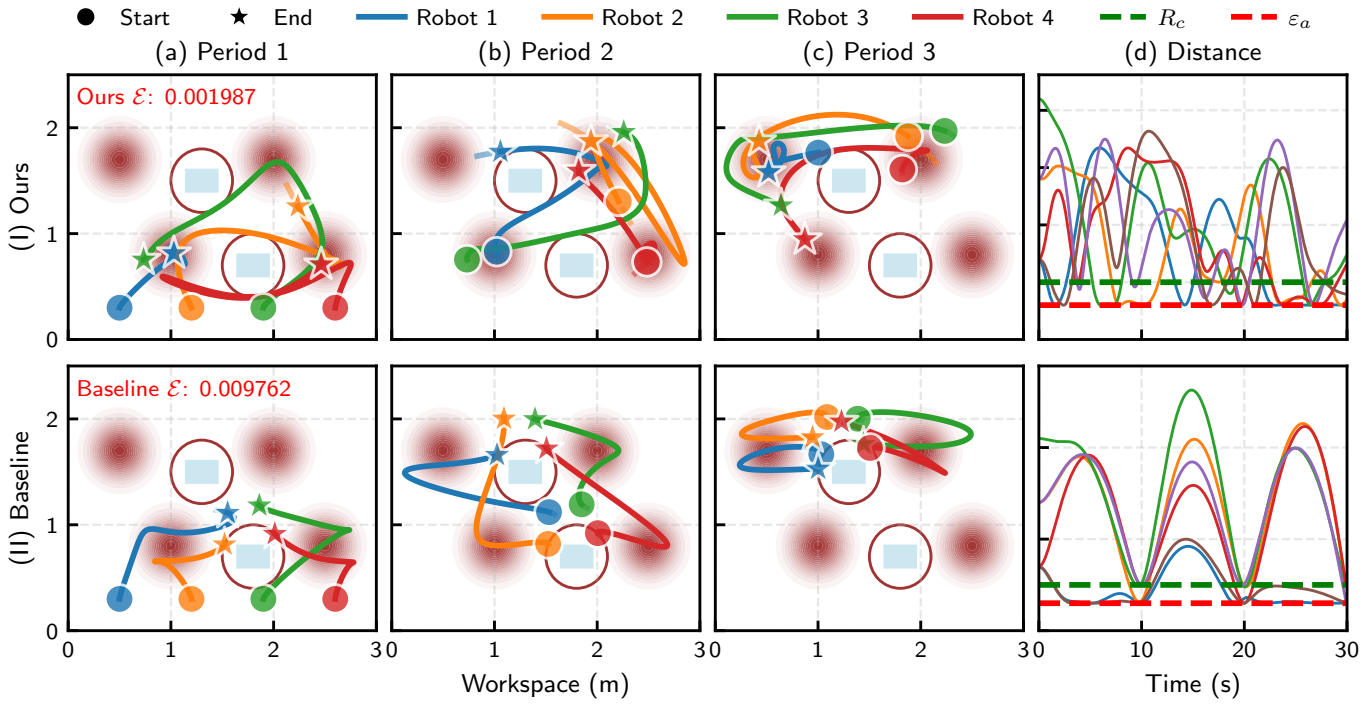


Fig. 9. The illustration of the connection strategies: (I) Ours – probabilistic connection, and (II) Baseline – periodic connection. Subfigures (a)-(c) show the robots' trajectories during each sub-period. Subfigure (d) illustrates the inter-distance between the robots. When the distance is less than $R_c$, the robots are connected. This figure demonstrates how the connection policies are designed to ensure that the robots maintain connectivity while navigating around obstacles. Both methods ensure that each pair of robots is connected at least once during each sub-period.

## VIII. Conclusion and Limitations

### A. Conclusion

This paper studies multi-robot ergodic search with intermittent connectivity maintenance. Unlike the existing work, this paper proposes a novel probabilistic measure of inter-robot connectivity based on the time-averaged statistics of the robots' trajectories. Based on the proposed measure, we formulate the MEC problem and derive the optimal conditions for the problem. We also develop IMEC, an iterative optimization algorithm to solve the MEC problem based on the augmented Lagrangian method and iterative LQR. The experiments verify the effectiveness of the proposed measure and the proposed planner in various information maps with varying parameters. Finally, the proposed planner is deployed on a real multi-drone system in a lab setting.

In particular, we observe from our results that, there is a positive correlation between the probabilistic measure of connectivity and the actual amount of connection time ratio in practice. Furthermore, using this probabilistic measure in ergodic search tends to give the planner more flexibility in

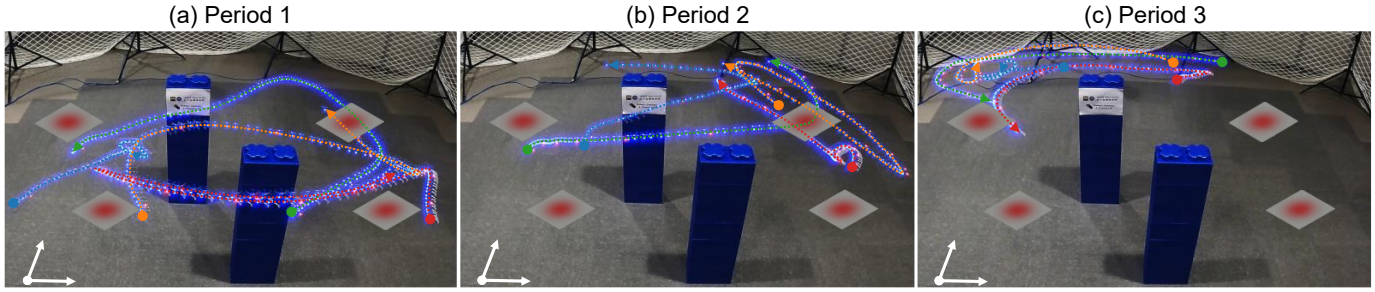


Fig. 10. Hardware experiment setup and results. The experimental platform consists of four drones in a motion-capture environment. (a)-(c) Snapshots of the drones executing the optimized trajectories during different sub-periods, demonstrating probabilistic connectivity maintenance during the ergodic search.

determining the location and time to build connections and thereby allows the planner to intelligently balance between ergodicity and connectivity maintenance in the long run.

### B. Limitations

This paper implements the algorithm in Python, which often takes a long runtime (sometimes more than a minute per run, especially when using a long planning horizon) and is not suitable for real-time on-board control. Combining it with receding horizon approaches and C++ implementation can potentially accelerate the computation and enable real-time control. Additionally, this paper simplifies the communication model as robots build connections and immediately complete data exchange upon gathering within a certain meeting radius. More realistic communication constraints, such as bandwidth and line-of-sight requirements, would be valuable to consider. Finally, the proposed planner is centralized in the sense that all robots' trajectories are available at any time. Future work includes developing the decentralized IMEC planner.

## References

[1] M. N. Rooker and A. Birk, "Multi-robot exploration under the constraints of wireless networking," *Control Engineering Practice*, vol. 15, no. 4, pp. 435–445, 2007.

[2] Y. Liu and G. Nejat, "Robotic urban search and rescue: A survey from the control perspective," *Journal of Intelligent & Robotic Systems*, vol. 72, pp. 147–165, 2013.

[3] E. U. Acar, H. Choset, A. A. Rizzi, P. N. Atkar, and D. Hull, "Morse decompositions for coverage tasks," *The international journal of robotics research*, vol. 21, no. 4, pp. 331–344, 2002.

[4] M. Santos, Y. Diaz-Mercado, and M. Egerstedt, "Coverage control for multirobot teams with heterogeneous sensing capabilities," *IEEE Robotics and Automation Letters*, vol. 3, no. 2, pp. 919–925, 2018.

[5] B. J. Julian, M. Angermann, M. Schwager, and D. Rus, "Distributed robotic sensor networks: An information-theoretic approach," *The International Journal of Robotics Research*, vol. 31, no. 10, pp. 1134–1154, 2012.

[6] W. Chen and L. Liu, "Pareto monte carlo tree search for multi-objective informative planning," in *Proceedings of Robotics: Science and Systems*, 2019.

[7] G. Mathew and I. Mezić, "Metrics for ergodicity and design of ergodic dynamics for multi-agent systems," *Physica D: Nonlinear Phenomena*, vol. 240, no. 4-5, pp. 432–442, 2011.

[8] L. M. Miller and T. D. Murphey, "Trajectory optimization for continuous ergodic exploration," in *2013 American Control Conference*. IEEE, 2013, pp. 4196–4201.

[9] G. De La Torre, K. Flaßkamp, A. Prabhakar, and T. D. Murphey, "Ergodic exploration with stochastic sensor dynamics," in *2016 American Control Conference (ACC)*. IEEE, 2016, pp. 2971–2976.

[10] Z. Ren, A. K. Srinivasan, B. Vundurthy, I. Abraham, and H. Choset, "A pareto-optimal local optimization framework for multiobjective ergodic search," *IEEE Transactions on Robotics*, vol. 39, no. 5, pp. 3452–3463, 2023.

[11] H. Coffin, I. Abraham, G. Sartoretti, T. Dillstrom, and H. Choset, "Multi-agent dynamic ergodic search with low-information sensors," in *2022 International Conference on Robotics and Automation (ICRA)*. IEEE, 2022, pp. 11 480–11 486.

[12] A. Mavrommati, E. Tzorakoleftherakis, I. Abraham, and T. D. Murphey, "Real-time area coverage and target localization using receding-horizon ergodic exploration," *IEEE Transactions on Robotics*, vol. 34, no. 1, pp. 62–80, 2017.

[13] I. Abraham and T. D. Murphey, "Decentralized ergodic control: distribution-driven sensing and exploration for multiagent systems," *IEEE Robotics and Automation Letters*, vol. 3, no. 4, pp. 2987–2994, 2018.

[14] D. Gkouletsos, A. Iannelli, M. H. de Badyn, and J. Lygeros, "Decentralized trajectory optimization for multi-agent ergodic exploration," *IEEE Robotics and Automation Letters*, vol. 6, no. 4, pp. 6329–6336, 2021.

[15] M. Guo and M. M. Zavlanos, "Distributed data gathering with buffer constraints and intermittent communication," in *2017 IEEE International Conference on Robotics and Automation (ICRA)*. IEEE, 2017, pp. 279–284.

[16] J. Banfi, N. Basilico, and F. Amigoni, "Multirobot reconnection on graphs: Problem, complexity, and algorithms," *IEEE Transactions on Robotics*, vol. 34, no. 5, pp. 1299–1314, 2018.

[17] G. A. Hollinger and S. Singh, "Multirobot coordination

with periodic connectivity: Theory and experiments," *IEEE Transactions on Robotics*, vol. 28, no. 4, pp. 967–973, 2012.

[18] R. Khodayi-mehr, Y. Kantaros, and M. M. Zavlanos, "Distributed state estimation using intermittently connected robot networks," *IEEE transactions on robotics*, vol. 35, no. 3, pp. 709–724, 2019.

[19] A. R. Da Silva, L. Chaimowicz, T. C. Silva, and M. A. Hsieh, "Communication-constrained multi-robot exploration with intermittent rendezvous," in *2024 IEEE/RSJ International Conference on Intelligent Robots and Systems (IROS)*. IEEE, 2024, pp. 3490–3497.

[20] Y. Kantaros, M. Guo, and M. M. Zavlanos, "Temporal logic task planning and intermittent connectivity control of mobile robot networks," *IEEE Transactions on Automatic Control*, vol. 64, no. 10, pp. 4105–4120, 2019.

[21] M. M. Zavlanos and G. J. Pappas, "Distributed connectivity control of mobile networks," *IEEE Transactions on Robotics*, vol. 24, no. 6, pp. 1416–1428, 2008.

[22] L. Sabattini, N. Chopra, and C. Secchi, "Decentralized connectivity maintenance for cooperative control of mobile robotic systems," *The International Journal of Robotics Research*, vol. 32, no. 12, pp. 1411–1423, 2013.

[23] W. Luo, S. Yi, and K. Sycara, "Behavior mixing with minimum global and subgroup connectivity maintenance for large-scale multi-robot systems," in *2020 IEEE International Conference on Robotics and Automation (ICRA)*. IEEE, 2020, pp. 9845–9851.

[24] M. A. Hsieh, A. Cowley, V. Kumar, and C. J. Taylor, "Maintaining network connectivity and performance in robot teams," *Journal of field robotics*, vol. 25, no. 1-2, pp. 111–131, 2008.

[25] F. Cladera, Z. Ravichandran, I. D. Miller, M. A. Hsieh, C. Taylor, and V. Kumar, "Enabling large-scale heterogeneous collaboration with opportunistic communications," in *2024 IEEE International Conference on Robotics and Automation (ICRA)*. IEEE, 2024, pp. 2610–2616.

[26] I. Abraham, A. Prabhakar, and T. D. Murphey, "An ergodic measure for active learning from equilibrium," *IEEE Transactions on Automation Science and Engineering*, vol. 18, no. 3, pp. 917–931, 2021.

[27] M. Sun, A. Gaggar, P. Trautman, and T. Murphey, "Fast ergodic search with kernel functions," *arXiv preprint arXiv:2403.01536*, 2024.

[28] C. Hughes, H. Warren, D. Lee, F. Ramos, and I. Abraham, "Ergodic trajectory optimization on generalized domains using maximum mean discrepancy," *arXiv preprint arXiv:2410.10599*, 2024.

[29] S. Ivić, B. Crnković, and I. Mezić, "Ergodicity-based cooperative multiagent area coverage via a potential field," *IEEE transactions on cybernetics*, vol. 47, no. 8, pp. 1983–1993, 2016.

[30] D. E. Dong, H. Berger, and I. Abraham, "Time-optimal ergodic search: Multiscale coverage in minimum time," *The International Journal of Robotics Research*, p. 02783649241273597, 2024.

[31] A. Seewald, C. J. Lerch, M. Chancán, A. M. Dollar, and I. Abraham, "Energy-aware ergodic search: Continuous exploration for multi-agent systems with battery constraints," in *2024 IEEE International Conference on Robotics and Automation (ICRA)*. IEEE, 2024, pp. 7048–7054.

[32] S. Shetty, J. Silvério, and S. Calinon, "Ergodic exploration using tensor train: Applications in insertion tasks," *IEEE Transactions on Robotics*, vol. 38, no. 2, pp. 906–921, 2021.

[33] A. Xu, B. Vundurthy, G. Gutow, I. Abraham, J. Schneider, and H. Choset, "Measure preserving flows for ergodic search in convoluted environments," *arXiv preprint arXiv:2409.09164*, 2024.

[34] B. L. Wellman, S. Dawson, J. de Hoog, and M. Anderson, "Using rendezvous to overcome communication limitations in multirobot exploration," in *2011 IEEE International Conference on Systems, Man, and Cybernetics*. IEEE, 2011, pp. 2401–2406.

[35] L. M. Miller, Y. Silverman, M. A. MacIver, and T. D. Murphey, "Ergodic exploration of distributed information," *IEEE Transactions on Robotics*, vol. 32, no. 1, pp. 36–52, 2015.

[36] L. S. Pontryagin, *Mathematical theory of optimal processes*. Routledge, 2018.

[37] D. P. Bertsekas, *Constrained optimization and Lagrange multiplier methods*. Academic press, 2014.

[38] T. A. Howell, B. E. Jackson, and Z. Manchester, "Altro: A fast solver for constrained trajectory optimization," in *2019 IEEE/RSJ International Conference on Intelligent Robots and Systems (IROS)*. IEEE, 2019, pp. 7674–7679.

[39] B. D. Anderson and J. B. Moore, *Optimal control: linear quadratic methods*. Courier Corporation, 2007.

[40] C. Llanes, Z. Kakish, K. Williams, and S. Coogan, "Crazysim: A software-in-the-loop simulator for the crazyflie nano quadrotor," in *2024 IEEE International Conference on Robotics and Automation (ICRA)*, 2024, pp. 12 248–12 254.

[41] W. Giernacki, M. Skwierczyński, W. Witwicki, P. Wroński, and P. Kozierski, "Crazyflie 2.0 quadrotor as a platform for research and education in robotics and control engineering," in *2017 22nd International Conference on Methods and Models in Automation and Robotics (MMAR)*. IEEE, 2017, pp. 37–42.

[42] J. A. Preiss, W. Honig, G. S. Sukhatme, and N. Ayanian, "Crazyswarm: A large nano-quadcopter swarm," in *2017 IEEE International Conference on Robotics and Automation (ICRA)*. IEEE, 2017, pp. 3299–3304.

[43] S. Macenski, T. Foote, B. Gerkey, C. Lalancette, and W. Woodall, "Robot operating system 2: Design, architecture, and uses in the wild," *Science robotics*, vol. 7, no. 66, p. eabm6074, 2022.

## APPENDIX A
## PROOFS

### A. Symmetry Property

From Eq. (4) and (5), we can express:

$$P_\infty(q^i, q^j) = \lim_{T\to\infty} P_c(q^i, q^j; 0, T) \tag{32a}$$

$$= \lim_{T\to\infty} \frac{1}{T^2} \int_0^T \int_0^T \gamma(q^i(t^i), q^j(t^j)) dt^j dt^i \tag{32b}$$

The symmetry property of Eq. (4) can be shown by the symmetry of the CIF (6). Under the bidirectional connectivity assumption (Assumption 1) that $q^j(t) \in \mathcal{S}(q^i(t)) \Leftrightarrow q^i(t) \in \mathcal{S}(q^j(t))$, we can infer that $\gamma(q^i(t^i), q^j(t^j)) = \gamma(q^j(t^j), q^i(t^i))$. This symmetry follows directly from the bidirectional property that $w^j \in S(w^i)$ implies $w^i \in S(w^j)$.

### B. Necessary Conditions of Optimality

Using the Hamiltonian (16), we can rewrite the Lagrange Function (14) as follows:

$$\mathcal{L} = \frac{r_\mathcal{E}}{2} s^T(T) Q_\mathcal{K} s(T) + \int_0^T H(x, s, u, \rho_x, \rho_s, \mu, t) - \rho_x^T(t)\dot{x}(t) - \rho_s^T(t)\dot{s}(t) dt \tag{33}$$

Here, the terminal cost term depends only on the auxiliary system state $s$ and does not depend on $x$. The Hamiltonian (16) is a function of the variables $x, s, u$ and the multipliers $\rho_x, \rho_s, \mu$, and the last two terms involve $\rho_x, \rho_s$ and the derivatives $\dot{x}, \dot{s}$.

We can derive the optimality conditions by taking the total variational derivative of Eq. (33) with respect to the states $x, s$, control $u$, multipliers $\rho_x, \rho_s, \mu$, and the derivatives $\dot{x}, \dot{s}$ as follows:

$$\begin{aligned}\delta\mathcal{L} = \frac{\partial \frac{r_\mathcal{E}}{2} s^T(T) Q_\mathcal{K} s(T)}{\partial s(T)} \delta s(T) + \int_0^T \Big\{ & \nabla_x^T H \delta x(t) \\ & + \nabla_s^T H \delta s(t) + \nabla_{\rho_x}^T H \delta \rho_x(t) + \nabla_{\rho_s}^T H \delta \rho_s(t) \\ & + \nabla_\mu^T H \delta \mu(t) + \nabla_u^T H \delta u(t) - \dot{x}^T(t) \delta \rho_x(t) \\ & - \rho_x^T(t) \delta \dot{x}(t) - \dot{s}^T(t) \delta \rho_s(t) - \rho_s^T(t) \delta \dot{s}(t) \Big\} dt \end{aligned} \tag{34}$$

Using integration by parts for $\rho_x^T(t)\delta\dot{x}(t)$ and $\rho_s^T(t)\delta\dot{s}(t)$ , we can simplify Eq. (34) as follows:

$$\begin{aligned}\delta\mathcal{L} = & \left( \frac{\partial \frac{r_\mathcal{E}}{2} s^T(T) Q_\mathcal{K} s(T)}{\partial s(T)} - \rho_s^T(T) \right) \delta s(T) - \rho_x^T(T) \delta x(T) \\ & + \int_0^T \Big\{ (\nabla_x^T H + \dot{\rho_x}^T(t)) \delta x(t) + (\nabla_s^T H + \dot{\rho_s}^T(t)) \delta s(t) \\ & + (\nabla_{\rho_x}^T H - \dot{x}^T(t)) \delta \rho_x(t) + (\nabla_{\rho_s}^T H - \dot{s}^T(t)) \delta \rho_s(t) \\ & + \nabla_\mu^T H \delta \mu(t) + \nabla_u^T H \delta u(t) \Big\} dt \end{aligned}$$

Let $\delta\mathcal{L} = 0$, we can get the conditions as shown in Eqs. (17).